pH-dependent structural dynamics of the neuropeptide Y in aqueous solution

Thi Hoa Nguyen,[1,2] Marc Spehr,[2,3] Ana-Nicoleta,[1,4*] Paolo Carloni[1,2,5*]

[1]Forschungszentrum Jülich, Computational Biomedicine, INM-9, Wilhelm-Johnen Straße, Jülich, Germany

[2]Research Training Group 2416 MultiSenses – MultiScales, RWTH Aachen University, 52074 Aachen, Germany

[3]RWTH Aachen University, Institute for Biology II, Department of Chemosensation, Worringerweg 3, D-52074 Aachen, Germany

[4]University of Bucharest, Faculty of Physics, Atomistilor 405, Magurele, Romania

[5]RWTH Aachen University, Molecular Science and Engineering, Aachen, Germany

*Correspondent authors

Abstract. Neuropeptide Y regulates key molecular processes in the brain. Its interaction with the cell membrane, fundamental for its function, is likely pH-dependent. Here, we perform constant pH simulations on the peptide in solution to investigate the impact of acidification on its protonation states and on its intra-molecular H-bond network. Our simulations point to a quite complex scenario at neutral or mildly acidic pH, where ionizable residues such as Asp, Glu, and His may exhibit fractional protonation states, affecting the conformational dynamics of the peptide in a non-trivial manner. Unanticipated structural dynamics emerge at low pH, where carboxyl groups are all neutral and histidine is di-protonated. Moreover, changes in protonation influence intra-molecular hydrogen bonding. Thus, using constant pH simulations could prove important to describe the structural peptide / protein dynamics at pH values that deviate from neutral.

Introduction

Neuropeptide Y (NPY) is a 36-residue peptide (Chart 1), abundant in mammalian brains.[1] As a neuromodulator it is involved in regulation of key processes such as memory formation and feeding.[2] In the hypothalamus, human NPY (hNPY) participates in cell signaling paths involved in delaying aging[3].[*] In these processes, hNPY may bind to the cell membrane[5] and/or to its target receptors[6] (such as the NPY Receptors 1 and 2, Y1R and Y2R)[7]. NPY-based peptide conjugates are being designed for

[*] The peptide can survive in post-mortem brain tissue at room temperature for up to 48 hours (4) Dawbarn, D.; Hunt, S. P.; Emson, P. C. Neuropeptide Y: regional distribution chromatographic characterization and immunohistochemical demonstration in post-mortem human brain. *Brain Research* **1984**, *296* (1), 168-173. DOI: https://doi.org/10.1016/0006-8993(84)90526-2, Beal, M. F.; Kowall, N. W.; Ellison, D. W.; Mazurek, M. F.; Swartz, K. J.; Martin, J. B. Replication of the neurochemical characteristics of Huntington's disease by quinolinic acid. *Nature* **1986**, *321* (6066), 168-171. DOI: 10.1038/321168a0.

cancer diagnosis and to deliver therapeutic cargo to cancer cells,[8] and a ligand for hY1R is of potential interest as nanocarrier to gliomas.[9]

pH is likely affecting peptide/membrane interactions substantially, as suggested by two observations: **(i)** Electrostatic interactions – which drive peptide binding to the membrane[10] – are weaker in buffer at pH 7.4 than in aqueous solution at pH 7.0.[11] **(ii)** The estimated free energy of peptide binding to a standard membrane is about 40% the energy calculated for a corresponding membrane with a high concentration of acidic lipids.[12] Thus, investigating the changes of protonation states of the system at different pH may provide a better understanding of membrane binding. Here, we begin to address this issue by performing constant pH molecular dynamics (CpHMD) simulations at both neutral and acidic pH. Considering our long-term goal to study peptide/membrane binding, we here perform CpHMD simulations on porcine (p)NPY, as its structure bound to micelles has been determined.[13]

In standard MD simulations, the protonation states of ionizable side chains are set up at the beginning. However, when pK_a values of residues are near the chosen pH (as is the case for histidine at physiological pH), both protonated and deprotonated states may coexist and their relative content may be altered by conformational rearrangement. In the CpHMD approach developed in[14], protonation states of ionizable groups are allowed to respond to changes in the chemical environment and the external pH.

Our calculations are based on the NMR structure of hNPY in solution at pH 3.2, which differs from pNPY only for the M17L substitution[15] (Chart 1). The peptide features an amphipathic, highly stable α-helical structure that extends from amino acid residues Pro13 to Thr32[13, 15], a flexible helix from Arg33 to Tyr36, and both N- and C-termini without ordered structures.

Chart 1. hNPY sequence. We consider residues 29 to 64 (without the signal peptide and C-terminal residues 65 to 97 of the full length NPY, UniProt entry A4D158), labeled 1 starting from the N-terminal Tyr residue. The C-terminus is amidated. hNPY and pNPY differ for their residue at position 16, which is Met in hNPY, and Leu in pNPY. Asp and Glu residues are colored red, Arg and Lys, blue, His, green, and Met17/Leu17, violet.

h(p)NPY: $Y_1PSK_4PD_6NPGE_{10}D_{11}APAE_{15}D_{16}M_{17}(L)AR_{19}YYSALR_{25}H_{26}YINLITR_{33}QR_{35}Y_{36}$

Methods

Structural model. The pNPY structure in solution was obtained from the hNPY NMR structure[15] by replacing M17 with a Leu residue. The Phyre2 web portal was used to model the mutant peptide,[16] using its "normal" modeling mode. His26 was described as $N\delta$ tautomer and the Glu and Asp residues (Chart 1) were considered negatively charged. The peptide was placed in the center of coordinates of

a box of 14,125 water molecules of 7.7 x 7.7 x 7.7 nm^3 with 0.15 M neutralizing NaCl using the CHARMM-GUI protocol[17].

Force-fields. We used the CHARMM36m force field parameters for the peptide and ions[18, 19], and the TIP3P water model[20]. For CpHMD simulations, we instead used the CHARMM22/CMAP force field for the protein[19, 21] and the CHARMM-modified TIP3P model for water[22]; this force field and water model are recommended for CpHMD simulations[23].

Protocol for standard MD simulations. The rigidBonds in NAMD[24] constrained all covalent bonds involving hydrogen (H) atoms. A timestep of 2fs was used. Constant temperature and pressure simulations were achieved by using a Nose-Hoover thermostat and a Nose-Hoover barostat, respectively.[25] Long-range electrostatics interactions were described with Particle Mesh Ewald (PME) using 1 Å of grid spacing. The cutoff radius of van der Waals interaction and short-range electrostatics was set to 1.2 nm.

The geometry of the peptide was first optimized by 15,000 steps of conjugate gradient.[26] It was then equilibrated for 10 ns *NVT* simulations with harmonic constraint constraints of 1.0 kcal/mol/$Å^2$ on the non-hydrogen atoms. All constraints were then switched off and computations continued for 500 ns of NPT MD.

Protocol for CpHMD simulations. These were based on one of the final MD snapshots of pNPY in water. To mimic the effect of gaining or releasing a proton to solution, the dummy ions were added to titratable residues (D/E/H) following the Constant pH User's Guide.[23]

The protocol for the simulations was identical to the one above except that here the SHAKE algorithm was used. The peptide was minimized by 10,000 steps of Steepest Descents (SD) and 5,000 steps of an adopted Newton-Raphson method (ABNR). This is the recommend minimization procedure for CHARMM.[23] The equilibration of NPY in water was carried out through 3 stages: **(i)** heating by 0.2 ns restrained MD from 5K to 303.15 K, in 100,000 steps with harmonic force constant of 1 kcal/mol/$Å^2$. **(ii)** The next four CpHMD equilibration steps were run for 0.2 ns in the *NVT* (constant number of atoms *N*, constant volume *V*, and constant temperature *T*) and *NPT* ensembles (constant pressure *P*), respectively, with protein heavy atoms restrained with harmonic force constant of 1.0; 0.5; 0.1 and 0 kcal/mol/$Å^2$. **(iii)** 40 ns in CpHMD production without constraints.

The number of coordinate sets where titratable residue i in the protonated or deprotonated were counted by defining as $\lambda_i < 0.1$ or $\lambda_i > 0.9$, respectively.

The unprotonated fraction of the residue (S_i) was calculated as:

$$S_i = \frac{N_i^{deprot}}{N_i^{deprot} + N_i^{prot}} \quad (1)$$

The pK_a values of titratable residues were obtained by fitting the S_i values at all simulation pH to generalized Henderson-Hasselbalch (HH) equation,

$$S_i = \frac{1}{1 + 10^{n(pK_{a,i} - pH)}} \quad (2)$$

where n is the Hill coefficient.

To investigate the convergence in protein titrations, we obtained the time series of the pK_a as well as the quality of fitting. Figures S14, S15, Table S1 in SI show the convergence of protein titration: the time series of the calculated pK_a values for pNPY from CpHMD simulations and unprotonated fraction best fits to the HH equation.

Analysis of protein bending and fluctuations. The Bendix code[27] was used to calculate the bending of the α-helix present in the peptide, and T-pad (the protein angular dispersion)[28] for the local fluctuations of the Cα atoms. The larger the T-pad value, the larger the corresponding fluctuation.[28]

H-bond network analyses. To study how the internal H-bond network of the peptide as a function of the pH, we used the graph-based algorithm and graphical user interface Bridge/Bridge2.[29, 30] Briefly, an H-bond graph consists of nodes, i.e., the H-bonding protein groups, and edges, i.e., the H-bond connections between these NPY groups. To understand how the sidechains, backbone groups, and water-mediated bridges, contribute to the intra-molecular H-bond network of pNPY, we separately computed three sets of H-bond graphs: 1) direct H-bonds of sidechains and backbone groups, and water-mediated bridges of these groups; 2) direct sidechain-sidechain H-bonds and water-mediated bridges between sidechains; 3) only the direct H-bonds between the sidechains. When included in the graph computation, the water-mediated bridges between protein groups had a maximum length of 3.0 Å, i.e., we considered water bridges with maximum three H-bonded waters. To identify H-bonds we used standard geometric criteria of H-bond distance ≤ 3.5 Å between the donor and acceptor heteroatoms, and H-bond angle ≤ 60º. The *occupancy* of an H-bond is given by the percentage of coordinate sets, of the total number of coordinate sets used for analyses, in which the H-bond criteria are met. Here, we used 2,000 equally spaced coordinate snapshots of 40 ns of each of the constant pH simulations. To simplify the display of the H-bond graphs, unless specified otherwise, we show only the H-bonds with a minimum H-bond occupancy of 50 %. This criterion is not unique and represents a compromise between the level of detail of the H-bond graphs, and the clarity of the H-bond connections of the titratable sidechains, which are the focus of our discussion. Moreover, the peptide is in aqueous solution and, as discussed below, most of the H-bonds of its protein-water H-bond network are water-mediated bridges. For unrelated proteins studied in aqueous solution we have found previously that bulk-exposed water bridges between carboxylic sidechains are short lived[31], and that at a minimum H-bond occupancy of 50 %, the H-bond networks from monomers of a homo-tetramer are very similar to each other[29]. On the other hand, we found that the H-bond network computed only for peptide sidechains, without water molecules, had relatively few H-bonds that mostly show lower occupancies. Consequently, for the H-bond network of the direct H-bonds, to

illustrate transient H-bonds sampled directly between the residues, we show the graphs at a minimum H-bond occupancy of 20 %.

Results

NPY in aqueous solution by standard MD. We first probed NPY conformational dynamics (in particular its H-bonding interactions) when all titratable sidechains have standard protonation states. As detailed below and illustrated in Figure 1, on the 500 ns timescale of our simulations, the peptide maintains a central α-helical segment, though there are fluctuations in the residues flanking this α-helical segment.

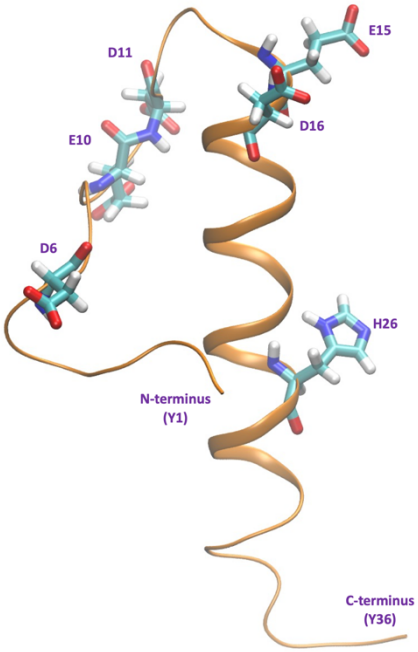

Figure 1. Peptide structure after 500 ns of standard MD simulations. The titratable residues, shown in ball and sticks, are considered in their fixed, standard protonation states. For clarity, water molecules and counterions are not shown.

The analysis of secondary structure elements as a function of simulation time (Figure S2) indicates that the helix is shortened relative to that revealed by NMR: it ranges from Ala12 to Arg35, sometimes from Glu15 to Thr32 or to Arg35. This could result, at least in part, 1) from pH differences among both systems: the NMR structure was solved at pH = 3.2, whereas in MD we consider the protonation states of the residues as to be consistent with a pH of 7.0; 2) from the change of one amino acid in the sequence. The maximum bending of the helical segment is also at a distinct residue and larger in MD than in the NMR structure: the largest bending of 60º, identified with Bendix, is at Ile28 (Figure S1, S2), as compared to 30º at Tyr21 in the NMR structure.

The backbone fluctuations, here quantified by T-pad values,[28] are shown in Figures 2 and S8. The helix-associated residues, from Ala14 to Thr32, have relatively small backbone fluctuations; this corresponds well to the helical structure solved by NMR.[15] The backbone fluctuations near the four Pro residues of the peptide (Chart 1) vary from 20^0 to 120^0. As expected, residues at the N- and C-termini (mostly coils, defined as conformations lacking secondary structure) have large backbone fluctuations.

In conclusion, our calculations suggest that: 1) the helix is somewhat shorter in regular MD than in the NMR structure at pH = 3.2; 2) as expected, the helix residues are far less flexible than the rest.

Constant pH MD simulations. Here, we compare MD simulations at constant pH; specifically, for simulation at pH 7.0, we compare our results with standard MD simulations.

(i) At *pH = 7.0* the helix shows small differences with that emerging from standard MD. It is slightly shorter (from Glu15 to Ile31/Thr32) and less flexible (see Figures 2, S3 S9, Table 1). The maximum bending angle of the helix is 48^0, located at Ile28 (Table 1). Moreover, the coil regions (from Tyr1 to Ala14 and from Thr32 to Tyr36) exhibit fluctuations similar to those in standard MD (Figures 2). The overall similarity with the standard MD may be caused by similarity in protonation states between both systems: all carboxyl groups are deprotonated and, only for short periods, His26 is deprotonated (Table 2).

(ii) At *pH = 6.0* the helix is slightly longer than in **(i)**: it ranges from Glu15 up to Thr32, at times up to Arg35 (Table 1, Figure S4). It is as flexible as the helix at pH = 7.0. This feature is common across all simulated pH values (Figures 2 and S10). The maximum bending angle is 55º, located at Thr32. The coil region from Tyr1 to Ala14 is less flexible than those in **(i)**, whereas the opposite is true for the Arg33-Tyr36 (Figures 2 and S10). Here, the Glu and Asp residues are ionized as in **(i),** but His26 is mostly positively charged during the simulations (Table 2).

(iii) At *pH = 5.0* the helix becomes slightly shorter than in **(ii)**, as it extends from Glu15 to Thr32 (Figure S5). The maximum bending angle of 22º occurs at Leu24 (Table 1). The coil regions decrease in flexibility upon transition from pH = 6.0 to pH = 5.0 (Figures 2 and S11). Some carboxyl groups are still ionized (those of Glu10, Glu15 and Asp16), whereas the remaining two aspartates (Asp6 and Asp11) spend significant periods in protonated state, consistent with calculated pKa values (Table 2). This shows that the environment modulates the pKa, affecting the protonation states of Asp and Glu residues in a non-trivial manner. At this pH, His26 is deprotonated, and, of course, it remains so by further lowering the pH.

(iv) At *pH = 4.0* the helix is shorter than that observed at pH = 5.0, as it extends only from Glu15 to Leu30, sometimes to Thr32 (Figure S6). The maximum bending angle of 30º occurs at Ile28 (Table 1). The coil regions have similar flexibility as those of **(iii)** (Figures 2 and S12). Asp6 and Asp11 now become fully protonated; Asp16 is still deprotonated as in **(iii)**, and the other carboxylic groups exhibit both protonation states (Table 2).

(v) At *pH = 3.0* the helix extends from Glu15 to Leu30 (at times up to Gln34, Figure S7). The maximum bending angle, 63º, is at Ile28 (Table 1). The coil regions are more flexible than in **(iv)** (Figures 2 and S13). All carboxyl groups but D16 are protonated most of the time (Table 2).

Table 1. Persistency of helical secondary structures during the dynamics of the simulated systems. The maximum bending angle values are calculated separately from the standard MD and the constant pH simulation trajectories. The data are obtained by inspection of Figures S2-S7.

Protonation states/ pH value	Boundaries of the α-helical segment		Maximum bending angle	
	Always	Transient extensions	Residue	Angle (º)
Standard MD simulation				
standard	Glu15-Ile31	Thr32-Arg35	Ile28	68^0
Constant pH MD simulations				
(i) (pH = 7)	Glu15-Ile31	Thr32	Ile28	48^0
(ii) (pH = 6)	Glu15-Thr32	Arg33-Arg35	Thr32	55^0
(iii) (pH = 5)	Glu15-Thr32	Arg33-Arg35	Leu24	22^0
(iv) (pH = 4)	Glu15-Leu30	Ile31-Thr32	Ile28	39^0
(v) (pH = 3)	Glu15-Leu30	Ile31-Gln34	Ile28	63^0

Table 2. pKa values (first row) and fraction (all other rows) of ionized carboxyl groups and neutral His26. We report the average values and their standard deviations.

	D6	E10	D11	E15	D16	H26
	4.618 (0.063)	3.560 (0.093)	5.183 (0.076)	3.719 (0.084)	3.031 (0.072)	6.251 (0.064)
pH3	0.043 (0.009)	0.237 (0.051)	0.013 (0.005)	0.233 (0.065)	0.483 (0.038)	0.000 (0.000)
pH4	0.194 (0.039)	0.717 (0.038)	0.084 (0.009)	0.592 (0.028)	0.895 (0.028)	0.009 (0.002)
pH5	0.704 (0.031)	0.934 (0.024)	0.432 (0.054)	0.944 (0.013)	0.992 (0.004)	0.070 (0.020)
pH6	0.956 (0.006)	0.993 (0.005)	0.806 (0.025)	0.990 (0.000)	0.990 (0.002)	0.392 (0.053)
pH7	0.990 (0.002)	1.000 (0.000)	0.972 (0.008)	1.000 (0.000)	1.000 (0.000)	0.797 (0.024)

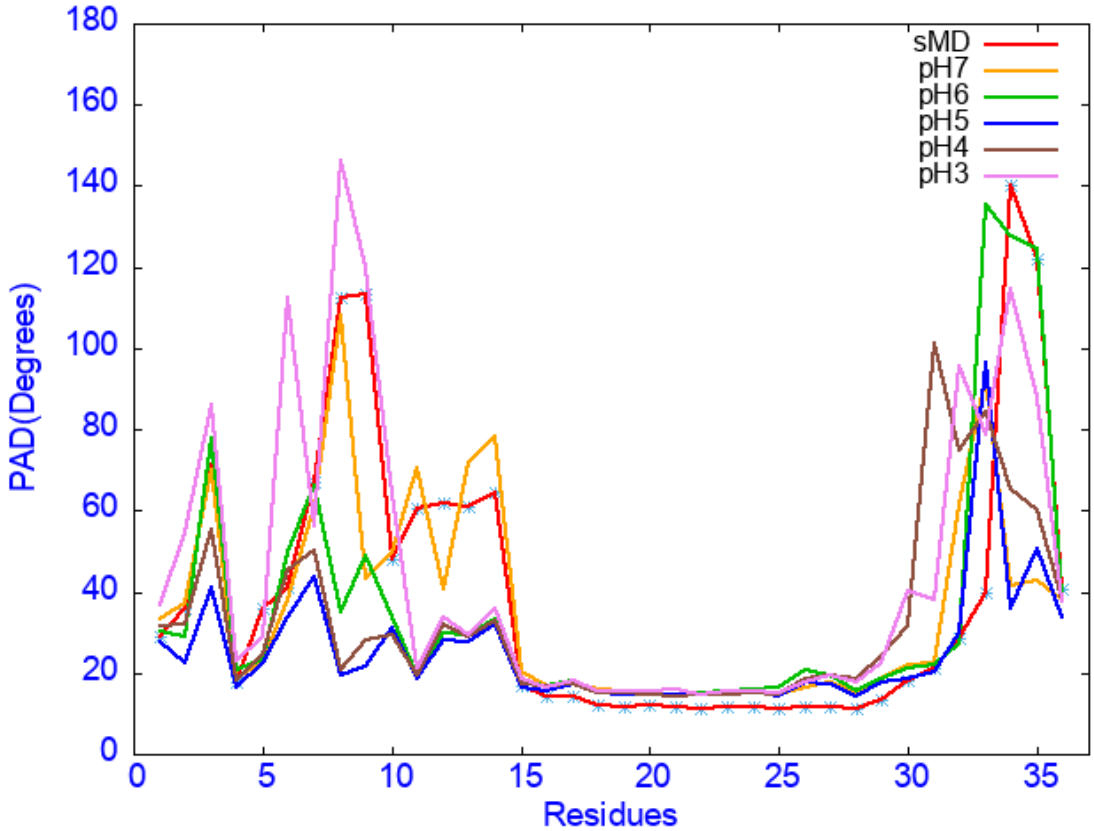

Figure 2. Fluctuations of **(i)-(v)** as quantified with T-pad. The larger the T-pad values, the larger the fluctuations of the residue backbone atoms. We compare T-pad values from simulations performed at different pH and regular MD.

pH-dependent H-bond network of pNPY in aqueous solution. The above changes in protonation states are accompanied by changes in the intra-molecular water-mediated H-bond network of the peptide sidechain and backbone groups (Figure 3). Our below discussion of the protein-water H-bond network is based on the H-bond graphs shown at a minimum H-bond occupancy of 50% (see Methods for details).

At pH = 3.0 and pH = 4.0, D6 connects only to S3 (Figures 3A, 3B, S16A&B). The H-bond connection between S3 and D6 is mostly direct, with a water bridge length <1.0 (Figure S17), and present at all studied pH values. In contrast, other connections between S3 and the remaining peptide appear pH dependent. For example, at pH = 3.0, pH = 6.0 and pH = 7.0, the S3-D6 local H-bond network lacks connections to the remaining of the H-bond graph shown at a minimum H-bond occupancy of 50% (Figure S16).

The sidechains of E10 and D11 bridge via 1-2 H-bonded waters at all pH values (Figures S17, S18, S19), but their connection to the remaining network depends on pH, that is, on preferred protonation states. These two residues are located on the relatively disordered N-terminal segment, where E10 water bridges to Y21 at all pH values (Figures 3, S17). In the H-bond graph, E10 connects to R25, except for pH = 3.0 and pH = 7.0, when both E10 and D11 prefer to be protonated and connected to

each other and, additionally, to Y21 and to the backbone of A12 (compare Figures 3A-D with Figure 3E). The finding that the H-bond connection between E10 and D11 is present in H-bond graphs computed with backbone groups (Figure 3) or for sidechains and water (Figure 4), but not when computed only for the sidechains (Figure 5) indicates that E10 and D11 connect via water-mediated bridging between their sidechains.

E15 and D16 bridge via ~2 H-bonded waters at all pH values except for pH = 5.0, where they connect to R19 mostly via direct H-bonds, which are present during 96-99% of the simulation (Figures S16, S17). However, the local H-bond network of E15 and D16 is rather similar regardless of pH, which is explained by the location of both residues, i.e., on the side of the helix away from the disordered N-terminal segment.

At all pH values except for pH = 5, H26 has mostly direct H-bonds with S22 and L30, and a short water bridge with N29 (Figure S17). The connection between H26 and N29 is absent at pH = 5 (Figure 3). Moreover, H26 is absent from the H-bond graphs computed for the sidechains, with (Figures 4, S18, S19) or without water bridges (Figure 5), which indicates that the H26 H-bond connections found in the graph that includes backbone groups are due to the latter.

The finding that there are few direct H-bonds between the sidechains of the peptide, and that most of these direct H-bonds are sampled with occupancies <50% (Figures 5, S20), is compatible with the peptide being in aqueous solution, where polar and charged sidechains prefer to interact with water. We note the strong pH dependence of the direct H-bonds between E15 and R19, which is sampled only at pH = 5.0, 6.0, and 7.0. At pH = 3.0 and pH = 4.0 E15 lacks direct sidechain H-bonds, and R19 H-bonds instead with D16 (Figure S20). Direct H-bonding between the sidechains of S3 and D6 is sampled only at pH = 6.0 and pH = 7.0 (Figure S20).

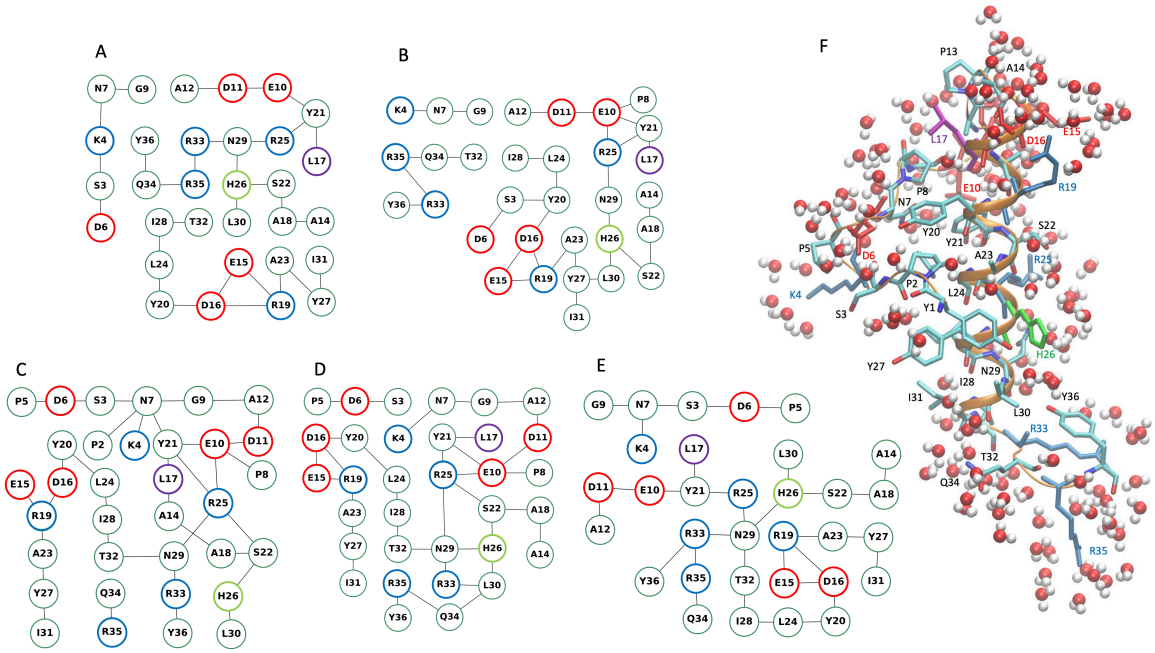

Figure 3. Dynamic protein-water H-bond network of NPY at different pH values. We used the Bridge2 graphical user interface to compute the H-bond network for protein sidechains, backbone groups, and water bridges with up to three H-bonded water molecules in a bridge. The minimum H-bond occupancy is 50%. (A-E) H-bond networks computed from simulations at pH = 3 (panel A), pH = 4 (panel B), pH = 5 (panel C), pH = 6 (panel D), and pH = 7 (panel E). (F) Molecular graphics of pNPY showing selected residues as bonds. The image is based on a coordinate snapshot from the simulation of pNPY at pH = 7. For clarity, H atoms of protein side chains are not shown. Supporting Information Figures S16 and S17 show these H-bond graphs with the average H-bond occupancy and, respectively, the average number of water molecules shown along the graph edges.

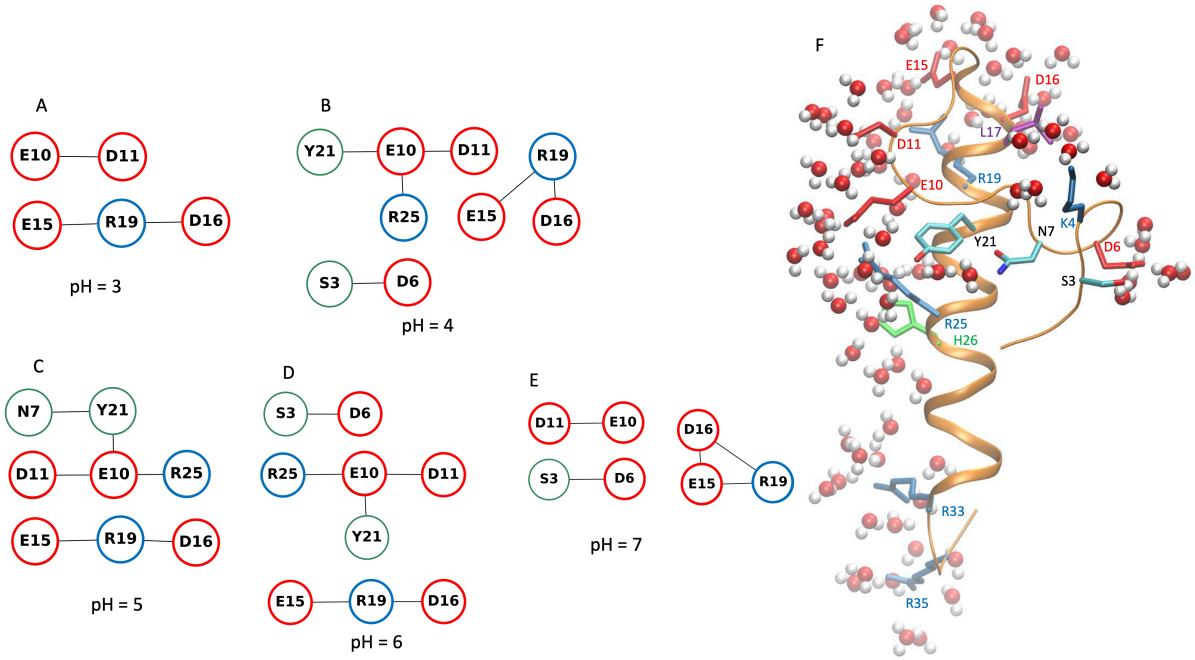

Figure 4 The water-mediated H-bond network of the sidechains, without backbone H-bonds. For clarity, we include only H-bonds with a minimum occupancy of 50%, and water bridges with up to three H-bonded water molecules. (A-E) H-bond networks of direct sidechain-sidechain and water-mediated bridges between sidechains computed from simulations at pH = 3 (panel A), pH = 4 (panel B), pH = 5 (panel C), pH = 6 (panel D), and pH = 7 (panel E). Supporting Information Figures S18 and S19 show, respectively, the average occupancies and the average length of the water bridges in the H-bond graphs presented in panels A-E. (F) Molecular graphics of pNPY showing selected sidechains and water molecules within 3.5 Å of side chain oxygen or nitrogen atoms.

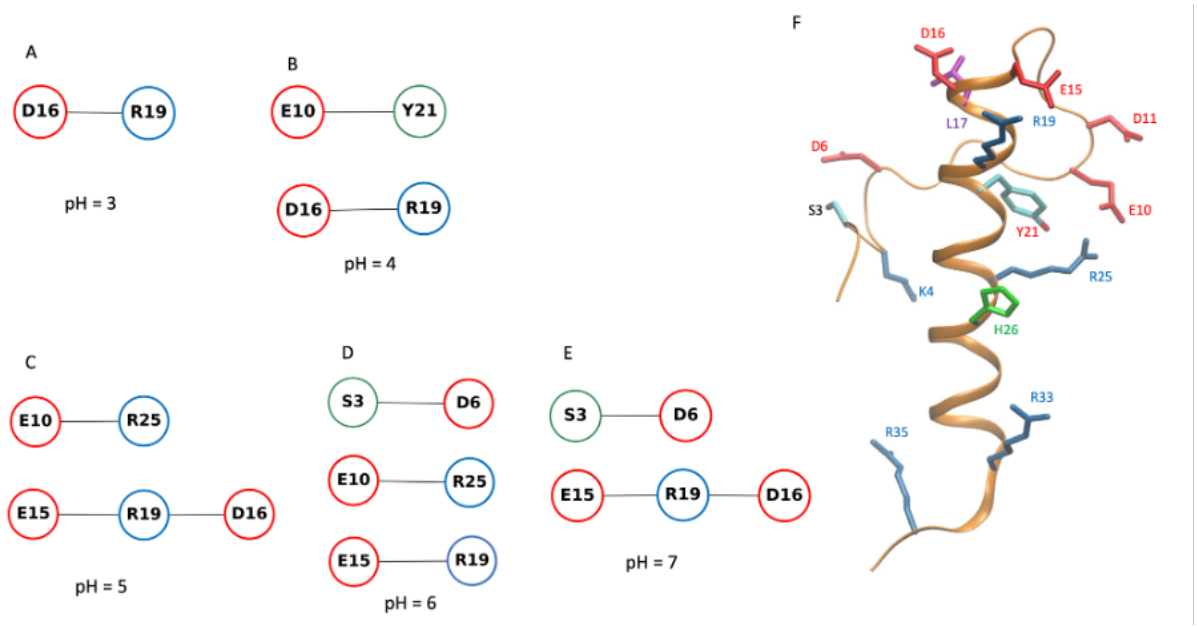

Figure 5. Direct H-bonds between sidechains of pNPY. The minimum H-bond occupancy shown is 20 %. H-bonds including backbone groups and water molecules were excluded from this graph computation. (A-E) H-bond networks computed for direct H-bonds. The graphs were computed from simulations at pH = 3 (panel B), pH = 4 (panel C), pH = 5 (panel D), pH = 6 (panel E), and pH = 7 (panel F). Figure S20 in the Supporting Information shows the corresponding graphs with the average occupancy in bridge indicated along the edges. (F) Molecular graphics of pNPY showing selected sidechains. For clarity, H atoms of protein side chains are not shown.

Discussions and Conclusions.

Our constant pH simulations on pNPY provide insight into complex peptide protonation patterns upon acidification, along its conformational changes. The simulation at pH 7.0 (or (**i**)) resembles standard MD, suggesting that the setup used in the latter (fixed deprotonated states for Asp/Glu and neutral His) is adequate to describe the peptide at neutral pH. However, the standard simulation does not take into account that His26 can, at times, be partly deprotonated[†]. Indeed, small differences are observed: in the simulation at pH 7.0, the helix is more rigid and at times longer at the C-term than the one from standard MD, while the maximum bending angle is smaller (Table 1, Figure 2).

More complex scenarios emerge for mildly acid pH: at pH = 6.0, His26 is mostly (but not completely) neutral, while for lower pH values (pH = 5.0, 4.0) it is the carboxyl groups that may be partially protonated, in a rather unpredictable manner. At this pH, His26 is always positively charged. Here, a standard MD with fixed protonation states is likely to be highly inadequate to describe the conformational dynamics of the peptide: The maximum bending angles and the coil regions of the peptide vary in a non-trivial manner upon acidification. At pH 3.0, instead, all carboxy group are protonated, as expected from the nominal pKa values of Asp and Glu in aqueous solution.

The analysis of the local H-bond networks of D6, E10/D11, and E15/D16 suggests that the pH-dependent change of the local H-bond network of a residue depends on the local molecular context, such that the response of the peptide's H-bond network to changes in the pH is more pronounced when the residue that changes protonation is part of a local intra-molecular H-bond cluster. We found a non-trivial pH dependence for both direct and water-mediated H-bonds of titratable sidechains.

In conclusion, we have presented a constant pH MD study on neuropeptide Y in neutral and acidic solutions, ranging from pH 7.0 to pH 3.0. The pKa values of Asp and Glu residues and the protonation states of ionizable residues vary widely and in non-trivial manner upon decrease of pH. Thus, performing CpHMD simulations might prove critical to accurately describe NPY binding with its cellular partners (including the Y1R/Y2R receptors and cellular membranes) at physiological and acidic pH.

References

[†] differences may also be caused by the difference in timescale investigated

(1) Tatemoto, K.; Carlquist, M.; Mutt, V. Neuropeptide Y—a novel brain peptide with structural similarities to peptide YY and pancreatic polypeptide. *Nature* **1982**, *296* (5858), 659-660. DOI: 10.1038/296659a0.
(2) Wettstein, J. G.; Earley, B.; Junien, J. L. Central nervous system pharmacology of neuropeptide Y. *Pharmacology & Therapeutics* **1995**, *65* (3), 397-414. DOI: https://doi.org/10.1016/0163-7258(95)98598-K.
(3) Aveleira, C. A.; Botelho, M.; Carmo-Silva, S.; Pascoal, J. F.; Ferreira-Marques, M.; Nóbrega, C.; Cortes, L.; Valero, J.; Sousa-Ferreira, L.; Álvaro, A. R.; et al. Neuropeptide Y stimulates autophagy in hypothalamic neurons. *Proceedings of the National Academy of Sciences* **2015**, *112* (13), E1642-E1651. DOI: 10.1073/pnas.1416609112 (acccessed 2024/10/01).
(4) Dawbarn, D.; Hunt, S. P.; Emson, P. C. Neuropeptide Y: regional distribution chromatographic characterization and immunohistochemical demonstration in post-mortem human brain. *Brain Research* **1984**, *296* (1), 168-173. DOI: https://doi.org/10.1016/0006-8993(84)90526-2. Beal, M. F.; Kowall, N. W.; Ellison, D. W.; Mazurek, M. F.; Swartz, K. J.; Martin, J. B. Replication of the neurochemical characteristics of Huntington's disease by quinolinic acid. *Nature* **1986**, *321* (6066), 168-171. DOI: 10.1038/321168a0.
(5) McLean, L. R.; Baron, B. M.; Buck, S. H.; Krstenansky, J. L. Lipid and membrane interactions of neuropeptide Y. *Biochimica et Biophysica Acta (BBA) - Biomembranes* **1990**, *1024* (1), 1-4. DOI: https://doi.org/10.1016/0005-2736(90)90201-X.
(6) Lerch, M.; Mayrhofer, M.; Zerbe, O. Structural Similarities of Micelle-bound Peptide YY (PYY) and Neuropeptide Y (NPY) are Related to their Affinity Profiles at the Y Receptors. *Journal of Molecular Biology* **2004**, *339* (5), 1153-1168. DOI: https://doi.org/10.1016/j.jmb.2004.04.032. Bettio, A.; Gutewort, V.; Pöppl, A.; Dinger, M. C.; Zschörnig, O.; Arnold, K.; Toniolo, C.; Beck-Sickinger, A. G. Electron paramagnetic resonance backbone dynamics studies on spin-labelled neuropeptide Y analogues. *Journal of Peptide Science* **2002**, *8* (12), 671-682. DOI: https://doi.org/10.1002/psc.428 (acccessed 2024/10/01).
(7) Larhammar, D. Structural diversity of receptors for neuropeptide Y, peptide YY and pancreatic polypeptide. *Regulatory Peptides* **1996**, *65* (3), 165-174. DOI: https://doi.org/10.1016/0167-0115(96)00110-3. Park, C.; Kim, J.; Ko, S.-B.; Choi, Y. K.; Jeong, H.; Woo, H.; Kang, H.; Bang, I.; Kim, S. A.; Yoon, T.-Y.; et al. Structural basis of neuropeptide Y signaling through Y1 receptor. *Nature Communications* **2022**, *13* (1), 853. DOI: 10.1038/s41467-022-28510-6. Tang, T.; Hartig, C.; Chen, Q.; Zhao, W.; Kaiser, A.; Zhang, X.; Zhang, H.; Qu, H.; Yi, C.; Ma, L.; et al. Structural basis for ligand recognition of the neuropeptide Y Y2 receptor. *Nature Communications* **2021**, *12* (1), 737. DOI: 10.1038/s41467-021-21030-9.
(8) Chastel, A.; Worm, D. J.; Alves, I. D.; Vimont, D.; Petrel, M.; Fernandez, S.; Garrigue, P.; Fernandez, P.; Hindié, E.; Beck-Sickinger, A. G.; et al. Design, synthesis, and biological evaluation of a multifunctional neuropeptide-Y conjugate for selective nuclear delivery of radiolanthanides. *EJNMMI Research* **2020**, *10* (1), 16. DOI: 10.1186/s13550-020-0612-8. Zwanziger, D.; Khan, I. U.; Neundorf, I.; Sieger, S.; Lehmann, L.; Friebe, M.; Dinkelborg, L.; Beck-Sickinger, A. G. Novel Chemically Modified Analogues of Neuropeptide Y for Tumor Targeting. *Bioconjugate Chemistry* **2008**, *19* (7), 1430-1438. DOI: 10.1021/bc7004297.
(9) Li, Y.; Pan, Y.; Wang, Y.; Jiang, Z.; Akakuru, O. U.; Li, M.; Zhang, X.; Yuan, B.; Xing, J.; Luo, L.; et al. A D-peptide ligand of neuropeptide Y receptor Y1 serves as nanocarrier traversing of the blood brain barrier and targets glioma. *Nano Today* **2022**, *44*, 101465. DOI: https://doi.org/10.1016/j.nantod.2022.101465.
(10) Thomas, L.; Scheidt, H. A.; Bettio, A.; Huster, D.; Beck-Sickinger, A. G.; Arnold, K.; Zschörnig, O. Membrane interaction of neuropeptide Y detected by EPR and NMR spectroscopy. *Biochimica et Biophysica Acta (BBA) - Biomembranes* **2005**, *1714* (2), 103-113. DOI: https://doi.org/10.1016/j.bbamem.2005.06.012.
(11) Dyck, M.; Kerth, A.; Blume, A.; Lösche, M. Interaction of the Neurotransmitter, Neuropeptide Y, with Phospholipid Membranes: Infrared Spectroscopic Characterization at

the Air/Water Interface. *The Journal of Physical Chemistry B* **2006**, *110* (44), 22152-22159. DOI: 10.1021/jp062537q.
(12) Thomas, L.; Scheidt, H. A.; Bettio, A.; Beck-Sickinger, A. G.; Huster, D.; Zschörnig, O. The interaction of neuropeptide Y with negatively charged and zwitterionic phospholipid membranes. *European Biophysics Journal* **2009**, *38* (5), 663-677. DOI: 10.1007/s00249-009-0423-3.
(13) Bader, R.; Bettio, A.; Beck-Sickinger, A. G.; Zerbe, O. Structure and Dynamics of Micelle-bound Neuropeptide Y: Comparison with Unligated NPY and Implications for Receptor Selection. *Journal of Molecular Biology* **2001**, *305* (2), 307-329. DOI: https://doi.org/10.1006/jmbi.2000.4264.
(14) Khandogin, J.; Brooks, C. L. Constant pH Molecular Dynamics with Proton Tautomerism. *Biophysical Journal* **2005**, *89* (1), 141-157. DOI: 10.1529/biophysj.105.061341 (acccessed 2024/10/01).
(15) Monks, S. A.; Karagianis, G.; Howlett, G. J.; Norton, R. S. Solution structure of human neuropeptide Y. *Journal of Biomolecular NMR* **1996**, *8* (4), 379-390. DOI: 10.1007/BF00228141.
(16) Kelley, L. A.; Mezulis, S.; Yates, C. M.; Wass, M. N.; Sternberg, M. J. E. The Phyre2 web portal for protein modeling, prediction and analysis. *Nature Protocols* **2015**, *10* (6), 845-858. DOI: 10.1038/nprot.2015.053.
(17) Jo, S.; Kim, T.; Im, W. Automated Builder and Database of Protein/Membrane Complexes for Molecular Dynamics Simulations. *PLOS ONE* **2007**, *2* (9), e880. DOI: 10.1371/journal.pone.0000880.
(18) Huang, J.; Rauscher, S.; Nawrocki, G.; Ran, T.; Feig, M.; de Groot, B. L.; Grubmüller, H.; MacKerell, A. D. CHARMM36m: an improved force field for folded and intrinsically disordered proteins. *Nature Methods* **2017**, *14* (1), 71-73. DOI: 10.1038/nmeth.4067. Best, R. B.; Zhu, X.; Shim, J.; Lopes, P. E. M.; Mittal, J.; Feig, M.; MacKerell, A. D., Jr. Optimization of the Additive CHARMM All-Atom Protein Force Field Targeting Improved Sampling of the Backbone ϕ, ψ and Side-Chain χ1 and χ2 Dihedral Angles. *Journal of Chemical Theory and Computation* **2012**, *8* (9), 3257-3273. DOI: 10.1021/ct300400x. MacKerell, A. D., Jr.; Feig, M.; Brooks, C. L. Improved Treatment of the Protein Backbone in Empirical Force Fields. *Journal of the American Chemical Society* **2004**, *126* (3), 698-699. DOI: 10.1021/ja036959e. Mackerell, A. D., Jr.; Feig, M.; Brooks, C. L., 3rd. Extending the treatment of backbone energetics in protein force fields: limitations of gas-phase quantum mechanics in reproducing protein conformational distributions in molecular dynamics simulations. *J Comput Chem* **2004**, *25* (11), 1400-1415. DOI: 10.1002/jcc.20065 From NLM.
(19) MacKerell, A. D., Jr.; Bashford, D.; Bellott, M.; Dunbrack, R. L., Jr.; Evanseck, J. D.; Field, M. J.; Fischer, S.; Gao, J.; Guo, H.; Ha, S.; et al. All-Atom Empirical Potential for Molecular Modeling and Dynamics Studies of Proteins. *The Journal of Physical Chemistry B* **1998**, *102* (18), 3586-3616. DOI: 10.1021/jp973084f.
(20) Jorgensen, W. L. Theoretical studies of medium effects on conformational equilibria. *The Journal of Physical Chemistry* **1983**, *87* (26), 5304-5314. DOI: 10.1021/j150644a002.
(21) Patel, S.; Mackerell Jr, A. D.; Brooks Iii, C. L. CHARMM fluctuating charge force field for proteins: II Protein/solvent properties from molecular dynamics simulations using a nonadditive electrostatic model. *Journal of Computational Chemistry* **2004**, *25* (12), 1504-1514. DOI: https://doi.org/10.1002/jcc.20077 (acccessed 2024/10/01).
(22) Brooks, B. R.; Brooks Iii, C. L.; Mackerell Jr, A. D.; Nilsson, L.; Petrella, R. J.; Roux, B.; Won, Y.; Archontis, G.; Bartels, C.; Boresch, S.; et al. CHARMM: The biomolecular simulation program. *Journal of Computational Chemistry* **2009**, *30* (10), 1545-1614. DOI: https://doi.org/10.1002/jcc.21287 (acccessed 2024/10/01).
(23) Henderson, J. A.; Liu, R.; Harris, J. A.; Huang, Y.; de Oliveira, V. M.; Shen, J. A Guide to the Continuous Constant pH Molecular Dynamics Methods in Amber and CHARMM [Article v1.0]. *Living J Comput Mol Sci* **2022**, *4* (1). DOI: 10.33011/livecoms.4.1.1563 From NLM.
(24) Phillips, J. C.; Braun, R.; Wang, W.; Gumbart, J.; Tajkhorshid, E.; Villa, E.; Chipot, C.; Skeel, R. D.; Kalé, L.; Schulten, K. Scalable molecular dynamics with NAMD. *Journal of*

Computational Chemistry **2005**, *26* (16), 1781-1802. DOI: https://doi.org/10.1002/jcc.20289 (acccessed 2024/10/01).
(25) Melchionna, S.; Ciccotti, G.; Lee Holian, B. Hoover NPT dynamics for systems varying in shape and size. *Molecular Physics* **1993**, *78* (3), 533-544. DOI: 10.1080/00268979300100371.
(26) Fletcher, R.; Reeves, C. M. Function minimization by conjugate gradients. *The Computer Journal* **1964**, *7* (2), 149-154. DOI: 10.1093/comjnl/7.2.149 (acccessed 10/1/2024).
(27) Dahl, A. C. E.; Chavent, M.; Sansom, M. S. P. Bendix: intuitive helix geometry analysis and abstraction. *Bioinformatics* **2012**, *28* (16), 2193-2194. DOI: 10.1093/bioinformatics/bts357 (acccessed 10/1/2024). Dalton, J. A. R.; Michalopoulos, I.; Westhead, D. R. Calculation of helix packing angles in protein structures. *Bioinformatics* **2003**, *19* (10), 1298-1299. DOI: 10.1093/bioinformatics/btg141 (acccessed 10/1/2024).
(28) Caliandro, R.; Rossetti, G.; Carloni, P. Local Fluctuations and Conformational Transitions in Proteins. *Journal of Chemical Theory and Computation* **2012**, *8* (11), 4775-4785. DOI: 10.1021/ct300610y.
(29) Siemers, M.; Bondar, A.-N. Interactive Interface for Graph-Based Analyses of Dynamic H-Bond Networks: Application to Spike Protein S. *Journal of Chemical Information and Modeling* **2021**, *61* (6), 2998-3014. DOI: 10.1021/acs.jcim.1c00306.
(30) Siemers, M.; Lazaratos, M.; Karathanou, K.; Guerra, F.; Brown, L. S.; Bondar, A.-N. Bridge: A Graph-Based Algorithm to Analyze Dynamic H-Bond Networks in Membrane Proteins. *Journal of Chemical Theory and Computation* **2019**, *15* (12), 6781-6798. DOI: 10.1021/acs.jctc.9b00697.
(31) Kemmler, L.; Ibrahim, M.; Dobbek, H.; Zouni, A.; Bondar, A.-N. Dynamic water bridging and proton transfer at a surface carboxylate cluster of photosystem II. *Physical Chemistry Chemical Physics* **2019**, *21* (45), 25449-25466, 10.1039/C9CP03926K. DOI: 10.1039/C9CP03926K.

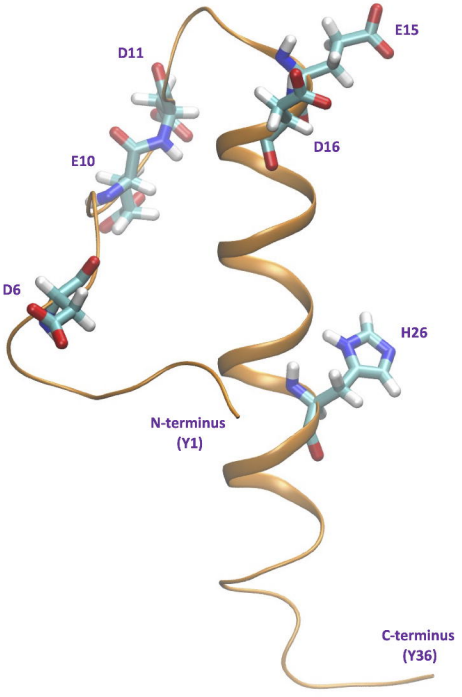
E15
D11
D16
E10
D6
H26
N-terminus
(Y1)
C-terminus
(Y36)

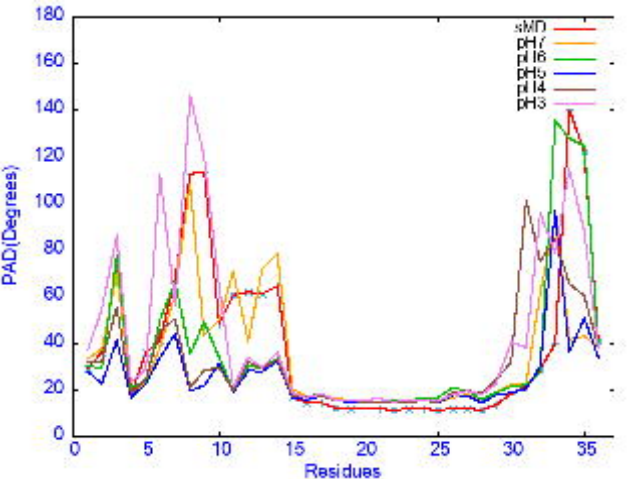
sMD
pH7
pH6
pH5
pH4
pH3
PAD(Degrees)
Residues
0
20
40
60
80
100
120
140
160
180
0
5
10
15
20
25
30
35

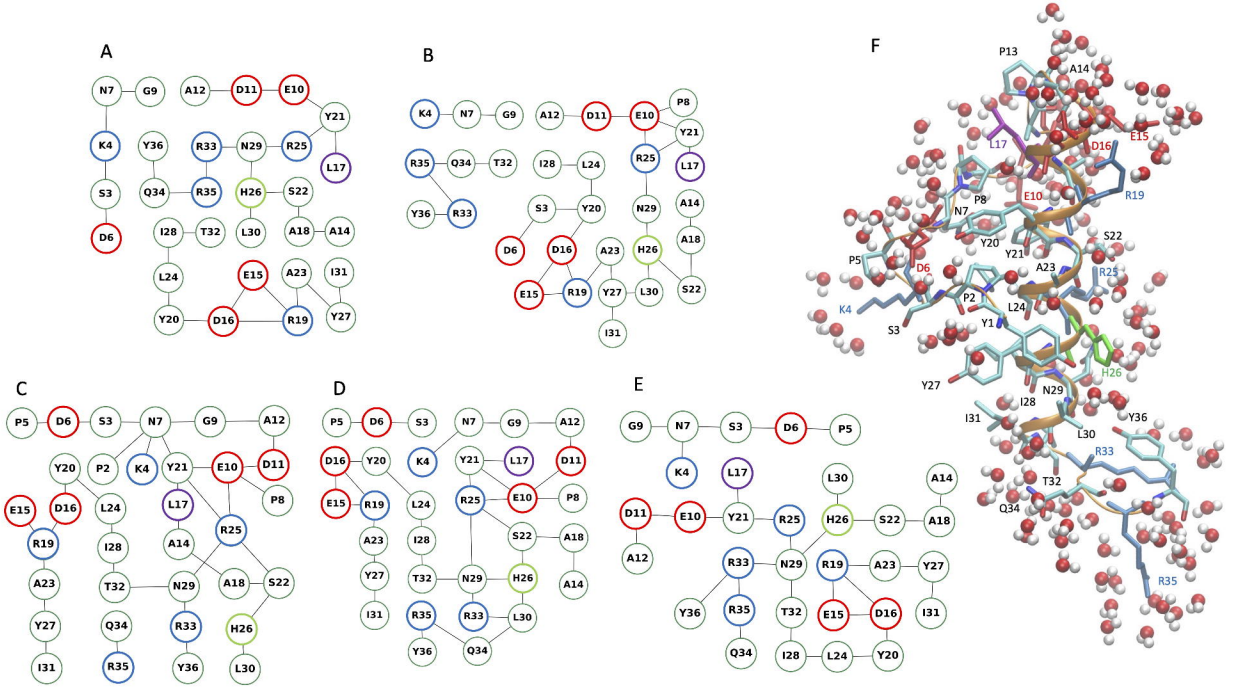
A
N7 G9 A12 D11 E10 Y21 K4 Y36 R33 N29 R25 L17 S3 Q34 R35 H26 S22 D6 I28 T32 L30 A18 A14 L24 E15 A23 I31 Y20 D16 R19 Y27
B
K4 N7 G9 A12 D11 E10 P8 Y21 R35 Q34 T32 I28 L24 R25 L17 Y36 R33 S3 Y20 N29 A14 D6 D16 A23 H26 A18 E15 R19 Y27 L30 S22 I31
C
P5 D6 S3 N7 G9 A12 Y20 P2 K4 Y21 E10 D11 E15 D16 L24 L17 P8 R19 I28 A14 R25 A23 T32 N29 A18 S22 Y27 Q34 R33 H26 I31 R35 Y36 L30
D
P5 D6 S3 N7 G9 A12 D16 Y20 K4 Y21 L17 D11 E15 R19 L24 R25 E10 P8 A23 I28 S22 A18 Y27 T32 N29 H26 A14 I31 R35 R33 L30 Y36 Q34
E
G9 N7 S3 D6 P5 K4 L17 L30 A14 D11 E10 Y21 R25 H26 S22 A18 A12 R33 N29 R19 A23 Y27 Y36 R35 T32 E15 D16 I31 Q34 I28 L24 Y20
F
P13 A14 L17 D16 E15 R19 E10 P8 N7 Y20 Y21 S22 P5 D6 A23 R25 K4 P2 L24 S3 Y1 H26 Y27 N29 I28 I31 Y36 L30 R33 T32 Q34 R35

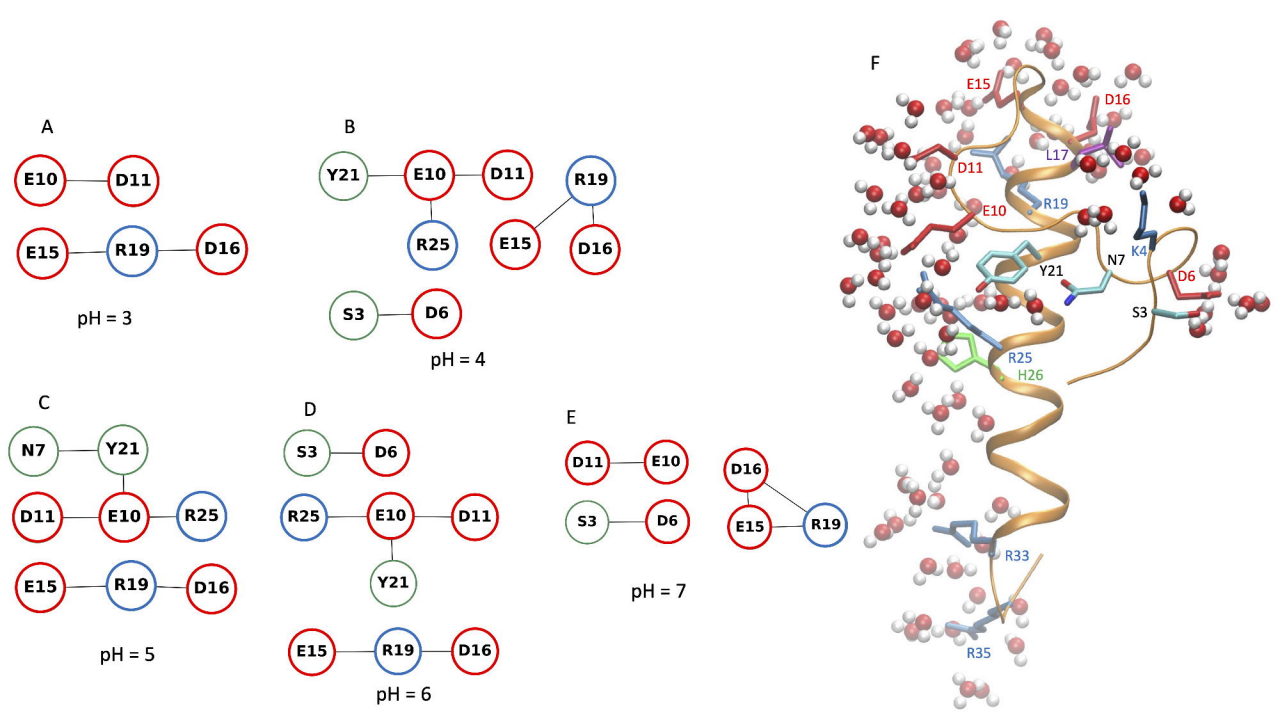
A
E10
D11
E15
R19
D16
pH = 3
B
Y21
E10
D11
R19
R25
E15
D16
S3
D6
pH = 4
C
N7
Y21
D11
E10
R25
E15
R19
D16
pH = 5
D
S3
D6
R25
E10
D11
Y21
E15
R19
D16
pH = 6
E
D11
E10
S3
D6
D16
E15
R19
pH = 7
F
E15
D16
L17
D11
R19
E10
K4
N7
Y21
D6
S3
R25
H26
R33
R35

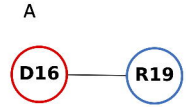
A
D16
R19
pH = 3

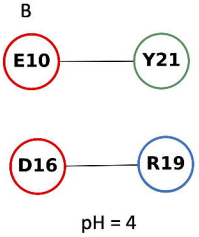
B
E10
Y21
D16
R19
pH = 4

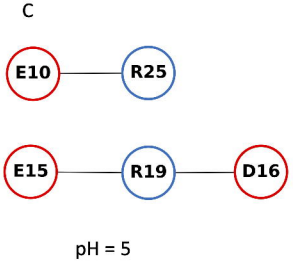
C
E10
R25
E15
R19
D16
pH = 5

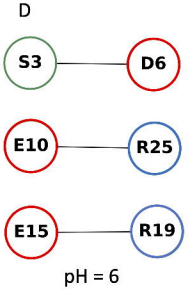
D
S3
D6
E10
R25
E15
R19
pH = 6

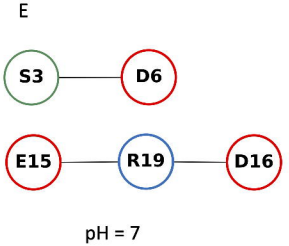
E
S3
D6
E15
R19
D16
pH = 7

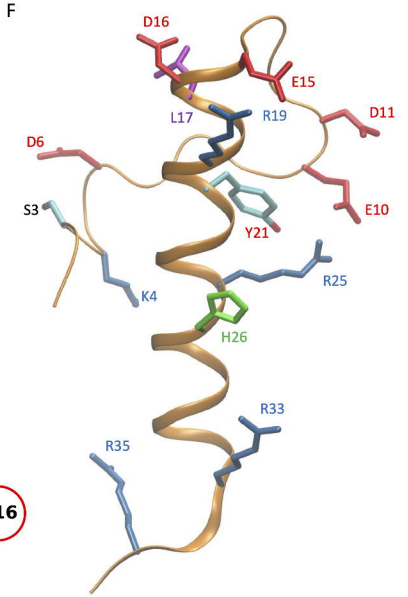
F
D16
E15
L17
R19
D11
D6
S3
Y21
E10
K4
R25
H26
R33
R35